// Weierstraß–Institut
für Angewandte Analysis und Stochastik

im Forschungsverbund Berlin e.V.

Preprint ISSN 0946 – 8633

Discrete Fourier transforms and their application to stress-strain problems in composite mechanics: A convergence study

C. M. Brown[1], Wolfgang Dreyer[2], Wolfgang H. Müller[3]

submitted: 30th October 2001

[1] Department of Mechanical and Chemical Engineering
Heriot-Watt University
Edinburgh EH14 4AS
Great Britain

[2] Weierstraß-Institut
für Angewandte Analysis
und Stochastik
Mohrenstraße 39
D – 10119 Berlin
Germany
E-Mail: dreyer@wias-berlin.de

[3] Technische Universität Berlin
Fakultät V
Institut für Mechanik
Einsteinufer 5
D – 10587 Berlin
E-Mail: Wolfgang.H.Mueller@TU-Berlin.de

Preprint No. 693
Berlin 2001

2000 *Mathematics Subject Classification.* 42B10, 45A05, 15A09, 74E30.

Key words and phrases. Discrete Fourier transforms, Neumann iteration, fixpoint theorem, composites.

Edited by
Weierstraß–Institut für Angewandte Analysis und Stochastik (WIAS)
Mohrenstraße 39
D — 10117 Berlin
Germany

Fax: + 49 30 2044975
E-Mail (X.400): c=de;a=d400-gw;p=WIAS-BERLIN;s=preprint
E-Mail (Internet): preprint@wias-berlin.de
World Wide Web: http://www.wias-berlin.de/

Abstract

We present in this paper a method for determining the convergence characteristics of the Neumann iterative solution of a discrete version of a second-type Fredholm equation. Implemented as the so-called "equivalent inclusion problem" within the context of mechanical stress/strain analysis, it allows the modeling of elastically highly heterogeneous bodies with the aid of Discrete Fourier Transforms (DFT). A method is developed with which we can quantify pre-analysis (*i.e.*, at iteration zero) the convergence behavior of the Neumann scheme depending on the choice of an auxiliary stiffness tensor, specifically for the linear-elastic case. It is shown that a careful choice of this tensor results in both guaranteed convergence and a smaller convergence radius for the solution. Furthermore, there is some indication that as the convergence radius decreases, the scheme may converge to a solution at a faster rate translating into an increase in computational efficiency.

1 Introduction

An important consideration during the design phase of composite materials is the determination of the overall, or effective, properties, which characterize the global behavior of the material under various load conditions. Although a suitable combination of both basis materials and geometry can yield highly specialized composites with vastly superior properties to the individual constituent phases, the determination of these properties by either analytical or numerical analysis can be a sizeable undertaking for all but the simplest of microstructural configurations.

Much work has been undertaken in the theory behind the calculation of effective constants, such as stiffnesses, yield stress, thermal expansion coefficients, or conductivities, by means of representing the material under investigation as a macroscopically homogeneous body within which the phase properties of the individual elements are "smeared out" (*homogenized*) over some Representative Volume Element (RVE). A huge variety of literature and examples of analytical results based on continuum mechanics is readily available (see, *e.g.*, Christensen, 1979, Hashin, 1962, 1964 or Lukkasen *et al.*, 1995).

Within the last few years, however, with the increasing availability of sufficiently powerful computing facilities and the motivation of an industry-wide drive to lower research and development costs, attention has turned to directly solving these so-called homogenization problems for more complex geometrical arrangements. This has been achieved by use of the Finite Element Method (FEM) by, amongst many others, Holmbom *et al.* (1992), Michel *et al.* (1999) and Hazotte *et al.* (1996). The application of this method has allowed the investigation of such arrangements as nonrectangular unit cells, multiple inclusions and of complex inclusion shape.

Recently, the Discrete Fourier Transform (DFT) has offered a viable and promising alternative to both FE and other methods as a basis for modeling mechanically and thermally mismatched materials. It has been used to model various heterogeneous materials problems by, for example, Moulinec and Suquet (1995, 1998) and also by the authors (*e.g.*, Müller, 1996, Dreyer and Müller, 2000, and Brown and Müller, 2000). In this context it should be mentioned that these papers concentrate on materials that are heterogeneous in terms of their elastic properties as well as their thermal expansion coefficients. Heterogeneites regarding thermal conductivity or electrical properties have not been covered so far. However, it should be noted that DFT is also able to effectively handle non-linear time-independent J_2 plasticity stress/strain analyses. This has been demonstrated in the papers by Moulinec and Suquet as well as in Herrmann *et al.* (1999).

As with any numerical technique, however, the parameters which influence the calculation must be carefully chosen in order that convergence of the solution is achieved and, in particular, special care must be taken when the level of elastic mismatch between the constituents in the material is high. To this end, in this paper we present a scheme for establishing convergence criteria for a DFT-based algorithm known as the *equivalent inclusion method* prior to the commencement of the analysis (*i.e.*, at iteration zero). The advantage of this scheme is obvious in that it allows us to quantify an appropriate choice of the parameters before undertaking computationally expensive calculations, and is shown to be both easy and efficient to implement in existing algorithms.

2 The Equivalent Inclusion Method

We consider now an RVE of a two-phase, linear elastic, heterogeneous material comprising an inclusion of arbitrary geometry and position embedded in a matrix such that the tractions and displacements are continuous over the interface between them (*i.e.*, they are perfectly bonded). The relationship between the stresses and strains in this RVE can immediately be defined for each point in space, $\underline{x}$, using Hooke's law as:

$$\sigma_{ij}(\underline{x}) = C_{ijkl}(\underline{x})(\varepsilon_{kl}(\underline{x}) - \varepsilon^*_{kl}(\underline{x})), \tag{2.1}$$

where σ_{ij} is the Cauchy stress tensor, ε_{kl} and ε^*_{kl} strains and the self-strains (or *eigenstrains*), respectively. $C_{ijkl}(\underline{x})$ is the stiffness tensor, which is assumed to be locally isotropic, and given as:

$$C^{+/-}_{ijkl} = \lambda^{+/-}\delta_{ij}\delta_{kl} + \mu^{+/-}(\delta_{ik}\delta_{jl} + \delta_{il}\delta_{jk}), \tag{2.2}$$

which, for a two phase material, can be written as the following combination of stiffness tensors of the matrix and the inclusion:

$$C_{ijkl}(\underline{x}) = C^{+}_{ijkl} - \theta(\underline{x})(C^{+}_{ijkl} - C^{-}_{ijkl}). \tag{2.3}$$

The variable $\theta(\underline{x})$ is known as the *shape function* and has the properties:

$$\theta(\underline{x}) = \begin{cases} 1 & \text{if } \underline{x} \in - \\ 0 & \text{if } \underline{x} \in + \end{cases}. \tag{2.4}$$

The two signs refer to the properties of the matrix phase (plus) and the inclusion phase (minus), respectively.

We can also state that the strains can be defined in terms of displacement gradients as follows:

$$\varepsilon_{kl} = \frac{1}{2}\left(\frac{\partial u_k}{\partial x_l} + \frac{\partial u_l}{\partial x_k}\right), \tag{2.5}$$

and require equilibrium of forces within the RVE:

$$\frac{\partial \sigma_{ij}}{\partial x_j} = 0. \tag{2.6}$$

Moreover, we assume periodic boundary conditions for all fields across the RVE and the objective now becomes to determine u_k or ε_{kl} from these equations. In order to arrive at a solution, we must first of all recognize that the stiffness tensor currently has a spatial dependence, which will now be eliminated using the equivalent inclusion technique (Mura, 1987). For this purpose, we introduce an *auxiliary strain field* $\varepsilon^{\mathrm{aux}}_{kl}$, which allows us to re-write Equation (2.1) as:

$$\sigma_{ij}(\underline{x}) = C^{\mathrm{aux}}_{ijkl}(\varepsilon_{kl}(\underline{x}) - \varepsilon^{*}_{kl}(\underline{x}) - \varepsilon^{\mathrm{aux}}_{kl}(\underline{x})), \tag{2.7}$$

where the superscript 'aux' denotes that the quantity has been modified to eliminate the spatial dependence of the stiffness tensor. Suitable choices of the *spatially constant* tensor $\underline{\underline{C}}^{\mathrm{aux}}$ will be discussed later.

Before proceeding, it is appropriate to recall Fourier's theorem in discrete form, which reads:

$$\hat{f}(\underline{s}) = Y\left[f(\underline{\alpha})\right] = \frac{1}{N^{d/2}} \sum_{\alpha_1=0}^{N-1} \cdots \sum_{\alpha_d=0}^{N-1} f(\underline{\alpha}) \exp\left(\mathrm{i}\frac{2\pi}{N}\underline{s} \cdot \underline{\alpha}\right) \tag{2.8}$$

with the inverse:

$$f(\underline{\alpha}) = Y^{-1}\left[\hat{f}(\underline{s})\right] = \frac{1}{N^{d/2}} \sum_{s_1=0}^{N-1} \cdots \sum_{s_d=0}^{N-1} \hat{f}(\underline{s}) \exp\left(-\mathrm{i}\frac{2\pi}{N}\underline{s} \cdot \underline{\alpha}\right), \tag{2.9}$$

where N is the number of discrete points per dimension d, and $\underline{s}$, $\underline{\alpha}$ are discrete position vectors in Fourier space and real space, respectively. This is depicted graphically in Figure 2.1 below for an RVE in real space. Periodicity conditions apply in all that follows:

$$f(\underline{\alpha}) = f(\underline{\alpha} + N\underline{r}), \quad r_i \in \{\cdots, -2, -1, -0, 1, 2, \cdots\}, \quad i \in \{1, \ldots, d\}. \quad (2.10)$$

It should be explicitly stated that all summations are *finite* and can be performed *exactly*, *e.g.*, by fast Fourier transform. The sums do *not* represent an approximation of the continuous infinite Fourier integrals.

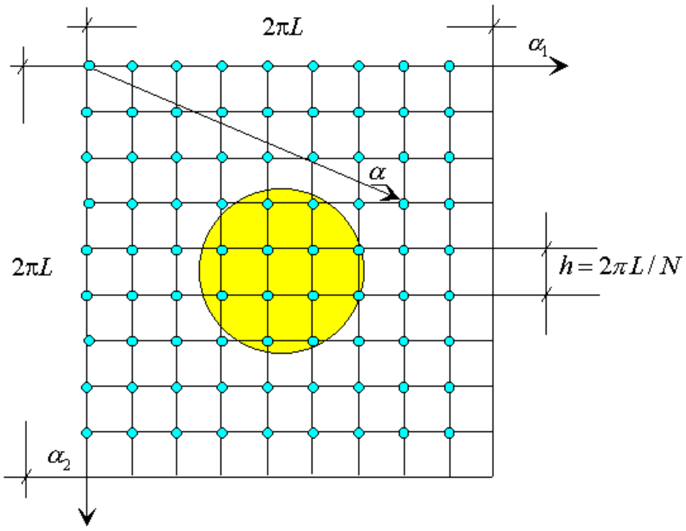

Figure 2.1: Discretization of the RVE in real space.

The following mappings hold for first and second order differentiation in Fourier space:

$$Y\left[\frac{\partial f}{\partial x_j}\right] = \xi_j Y(f(\underline{\alpha})) + O(h^2), \qquad Y\left[\frac{\partial^2 f}{\partial x_j \partial x_l}\right] = \xi_{jl} Y(f(\underline{\alpha})) + O(h^2), \quad (2.11)$$

where $\mathrm{i} = \sqrt{-1}, h = \frac{2\pi L}{N}$, and[1]:

$$\xi_j = -\mathrm{i}\frac{1}{h}\sin\left(\frac{2\pi}{N}s_j\right), \qquad \xi_{\underline{i}\,\underline{i}} = \frac{2}{h^2}\left(\cos\left(\frac{2\pi}{N}s_i\right) - 1\right), \quad (2.12)$$

$$\xi_{ij} = \frac{1}{2h^2}\left(\cos\left(\frac{2\pi}{N}(s_i + s_j)\right) - \cos\left(\frac{2\pi}{N}(s_i - s_j)\right)\right), \quad i \neq j. \quad (2.13)$$

If we now substitute Equations (2.5) and (2.6) into Equation (2.7), it can be shown (*e.g.*, Dreyer & Müller, 2000) that the localized strains are given by:

$$\varepsilon_{ij}(\underline{\alpha}) = Y^{-1}\left[\hat{A}^{\mathrm{aux}}_{ijkl}(\underline{s})\hat{\varepsilon}^{*}_{kl}(\underline{s})\right](\underline{\alpha}) + Y^{-1}\left[\hat{A}^{\mathrm{aux}}_{ijkl}(\underline{s})\hat{\varepsilon}^{\mathrm{aux}}_{kl}(\underline{s})\right](\underline{\alpha}) + \varepsilon^0_{ij}, \quad (2.14)$$

[1] An underlined index indicates that the Einstein summation convention does not apply.

where :

$$\hat{A}^{\text{aux}}_{ijkl}(\underline{s}) = \begin{cases} 0, & \underline{s} = \underline{0}, \\ \frac{1}{2}\left(\xi_i(\underline{s})M^{-1}_{jo}(\underline{s}) + \xi_j(\underline{s})M^{-1}_{io}(\underline{s})\right) C^{\text{aux}}_{opkl}\xi_p, & \underline{s} \neq \underline{0}, \end{cases} \tag{2.15}$$

$$M_{ik}(\underline{s}) = C^{\text{aux}}_{ijkl}\xi_{jl}(\underline{s}), \tag{2.16}$$

and ε^0_{ij} are the external overall strains, applied to the RVE, *i.e.*, constant in space. It should be noted (Michel *et al.*, 1999) that these are identical to the average strains acting on the RVE. If we now equate Equations (2.7) and (2.1) we may write, after appropriate substitution of Equation (2.3), that:

$$C^{\text{aux}}_{ijkl}\varepsilon^{\text{aux}}_{kl}(\underline{\alpha}) = \beta(\underline{\alpha})\left(C^{+}_{ijkl} - C^{-}_{ijkl}\right)\left(\varepsilon_{kl}(\underline{\alpha}) - \varepsilon^{*}_{kl}(\underline{\alpha}) + \varepsilon^{0}_{kl}\right), \tag{2.17}$$

where $\beta(\underline{\alpha})$ is a spatially dependent quantity, which is dependent on the choice of the C^{aux} tensor. Table 2.1 below shows the three most obvious choices of this tensor, and the corresponding values of the real quantity $\beta(\underline{\alpha})$.

$\underline{\underline{C}}^{\text{aux}}$	$\beta(\underline{\alpha})$	use for
$\underline{\underline{C}}^{+}$	$\theta(\underline{\alpha})$	stiff matrix, soft inclusion
$\underline{\underline{C}}^{-}$	$\theta(\underline{\alpha}) - 1$	soft matrix, hard inclusion
$\frac{1}{2}\left(\underline{\underline{C}}^{+} + \underline{\underline{C}}^{-}\right)$	$\frac{1}{2}\left(2\theta(\underline{\alpha}) - 1\right)$	any case

Table 2.1 Choices of the $\underline{\underline{C}}^{\text{aux}}$-tensor, and corresponding values of $\beta(\underline{\alpha})$.

On insertion of Equation (2.14) into Equation (2.17), and inverting the C^{aux} tensor, we can write Equation (2.17) as follows:

$$\varepsilon^{\text{aux}}_{ij}(\underline{\alpha}) = \beta(\underline{\alpha})\lambda_{ijrs}\left(Y^{-1}\left[\hat{A}^{\text{aux}}_{rsmn}\hat{\varepsilon}^{*}_{mn}\right](\underline{\alpha}) + Y^{-1}\left[\hat{A}^{\text{aux}}_{rsmn}\hat{\varepsilon}^{\text{aux}}_{mn}\right](\underline{\alpha}) - \varepsilon^{*}_{rs}(\underline{\alpha}) + \varepsilon^{0}_{rs}\right). \tag{2.18}$$

Also, in context with Equation (2.18), we can introduce the following analytical results to simplify subsequent calculations, which will be required in the calculation of convergence properties:

$$(C^{\text{aux}})^{-1}_{klrs} = A\delta_{kl}\delta_{rs} + B(\delta_{kr}\delta_{ls} + \delta_{ks}\delta_{lr}), \tag{2.19}$$

with (for plane strain):

$$A = -\frac{\lambda^{\text{aux}}}{4\mu^{\text{aux}}(\lambda^{\text{aux}} + \mu^{\text{aux}})}, \quad B = \frac{1}{4\mu^{\text{aux}}}, \tag{2.20}$$

and also:

$$\begin{aligned}
\lambda_{ijrs} &= (C^{\text{aux}})^{-1}_{ijop}(C^{+}_{oprs} - C^{-}_{oprs}) \\
&= 2\left[\lambda^{+}(A+B)\Big(1-\frac{\lambda^{-}}{\lambda^{+}}\Big) + A\mu^{+}\Big(1-\frac{\mu^{-}}{\mu^{+}}\Big)\right]\delta_{ij}\delta_{rs} + \\
&\quad 2B\mu^{+}\Big(1-\frac{\mu^{-}}{\mu^{+}}\Big)(\delta_{ir}\delta_{js}+\delta_{is}\delta_{jr}).
\end{aligned} \tag{2.21}$$

Moreover, for plane strain the symbols $\hat{A}^{\text{aux}}_{mnkl}$ of Equation (2.15) can be detailed as follows:[2]

$$\begin{aligned}
\hat{A}^{\text{aux}}_{mnkl} =& \frac{1}{2}\Big\{\lambda^{\text{aux}}\left[2A_1\xi_m\xi_n\delta_{kl} + A_2(\xi_m\xi_{np}+\xi_n\xi_{mp})\xi_p\delta_{kl}\right] + \\
& \mu^{\text{aux}}\Big[A_1(\xi_m\delta_{nk}\xi_l + \xi_m\delta_{nl}\xi_k + \xi_n\delta_{mk}\xi_l + \xi_n\delta_{ml}\xi_k) + \\
& A_2(\xi_m\xi_{nk}\xi_l + \xi_m\xi_{nl}\xi_k + \xi_n\xi_{mk}\xi_l + \xi_n\xi_{ml}\xi_k)\Big]\Big\}
\end{aligned} \tag{2.22}$$

with:

$$\begin{aligned}
A_1 &= \frac{(\lambda^{\text{aux}}+2\mu^{\text{aux}})(\xi_{11}+\xi_{22})}{\mu^{\text{aux}}(\lambda^{\text{aux}}+2\mu^{\text{aux}})(\xi_{11}+\xi_{22})^2 + (\lambda^{\text{aux}}+\mu^{\text{aux}})^2(\xi_{11}\xi_{22}-\xi_{12}^2)}, \\
A_2 &= -\frac{\lambda^{\text{aux}}+\mu^{\text{aux}}}{\mu^{\text{aux}}(\lambda^{\text{aux}}+2\mu^{\text{aux}})(\xi_{11}+\xi_{22})^2 + (\lambda^{\text{aux}}+\mu^{\text{aux}})^2(\xi_{11}\xi_{22}-\xi_{12}^2)}.
\end{aligned} \tag{2.23}$$

A solution of Equation (2.18) is achieved using an iterative scheme of the Neumann type as follows:

$$\begin{aligned}
\overset{(n+1)}{\varepsilon^{\text{aux}}_{ij}}(\underline{\alpha}) =& \beta(\underline{\alpha})\lambda_{ijrs}\times \\
& \left(Y^{-1}\left[\hat{A}^{\text{aux}}_{rsmn}\hat{\varepsilon}^{*}_{mn}\right](\underline{\alpha}) + Y^{-1}\left[\hat{A}^{\text{aux}}_{rsmn}\overset{(n)}{\hat{\varepsilon}^{\text{aux}}_{mn}}\right](\underline{\alpha}) - \varepsilon^{*}_{rs}(\underline{\alpha}) + \varepsilon^{0}_{rs}\right)
\end{aligned} \tag{2.24}$$

with the starting condition:

$$\overset{(0)}{\varepsilon^{\text{aux}}_{kl}}(\underline{\alpha}) = 0. \tag{2.25}$$

In fact, choosing this approach is not too surprising since Equation (2.18) is the discrete analogue of a Fredholm integral equation of the second kind, which arises if the DFTs are substituted by continuous Fourier integrals. Such integral equations, however, are typically solved by means of successive substitution of the kernel functions (see *e.g.*, Porter and Stirling, 1990, pp. 78, Moiseiwitsch, 1977, pp. 43, or, most explicitly, Bronstein-Semendjajew, 1976, pp. 539), *i.e.*, using the Neumann technique.

[2] This expression is obtained from the basic definitions shown in Equations (2.2), (2.12), (2.13), (2.16) and Table 2.1 if specialized to two spatial dimensions. As it will be shown in the appendix the indices m, n, k, l will have to run only from 1 to 2.

3 Determination of the Auxiliary Strain Using Banach's Fixpoint Theorem

In this section we shall investigate the convergence of the scheme presented in Equations (2.24), (2.25) for the auxiliary strain. To obtain a better overview we rewrite Equation (2.18) to reveal that it is a (complex) linear system of equations:

$$\varepsilon_{ij}^{\mathrm{aux}}(\underline{\alpha}) = \sum_{\alpha_1'=0}^{N-1} \cdots \sum_{\alpha_d'=0}^{N-1} K_{ijmn}(\underline{\alpha}, \underline{\alpha}') \varepsilon_{mn}^{\mathrm{aux}}(\underline{\alpha}') + f_{ij}(\underline{\alpha}) \tag{3.1}$$

using the contraction:

$$K_{ijmn}(\underline{\alpha}, \underline{\alpha}') = \beta(\underline{\alpha}) \lambda_{ijrs} k_{rsmn}(\underline{\alpha}, \underline{\alpha}'), \tag{3.2}$$

where $\beta(\underline{\alpha})$ and λ_{ijrs} stem from Table 2.1 and Equation (2.21), respectively. Moreover:

$$k_{ijmn}(\underline{\alpha}, \underline{\alpha}') = \frac{1}{N^d} \sum_{s_1=0}^{N-1} \cdots \sum_{s_d=0}^{N-1} \hat{A}_{ijmn}^{\mathrm{aux}}(\underline{s}) \exp\left(-\mathrm{i}\frac{2\pi}{N} \underline{s} \cdot (\underline{\alpha} - \underline{\alpha}')\right), \tag{3.3}$$

and:

$$f_{ij}(\underline{\alpha}) = \lambda_{ijrs} \beta(\underline{\alpha}) \left(Y^{-1}\left[\hat{A}_{rsmn}^{\mathrm{aux}} \hat{\varepsilon}_{mn}^{*}\right](\underline{\alpha}) - \varepsilon_{rs}^{*}(\underline{\alpha}) + \varepsilon_{rs}^{0}\right). \tag{3.4}$$

A further simplification results if we use Equation (2.9) for rewriting Equation (3.3):

$$k_{ijmn}(\underline{\alpha}, \underline{\alpha}') = \frac{1}{N^{d/2}} A_{ijmn}^{\mathrm{aux}}(\underline{\alpha} - \underline{\alpha}') \tag{3.5}$$

so that:

$$K_{ijmn}(\underline{\alpha}, \underline{\alpha}') = \beta(\underline{\alpha}) \lambda_{ijrs} \frac{1}{N^{d/2}} A_{rsmn}^{\mathrm{aux}}(\underline{\alpha} - \underline{\alpha}'). \tag{3.6}$$

Consequently, for a given fixed N the components of the auxiliary strain are determined by a linear algebraic system. However, finding the solution of Equation (3.1) by means of Cramer's rule is numerically very intensive, in particular if the presented problem couples to a time-dependent diffusion problem and then needs to be solved in every time-step (*cf.*, Dreyer and Müller, 2000).

Therefore we will determine the components of the auxiliary stain from the system of Equations (3.1) iteratively, as indicated in Equations (2.24), (2.25), *i.e.*, using our new nomenclature:

$$\begin{aligned}
&\overset{(0)}{\varepsilon_{ij}^{\mathrm{aux}}}(\underline{\alpha}) = 0, \\
&\overset{(n+1)}{\varepsilon_{ij}^{\mathrm{aux}}}(\underline{\alpha}) = \sum_{\alpha_1'=0}^{N-1} \cdots \sum_{\alpha_d'=0}^{N-1} K_{ijmn}(\underline{\alpha}, \underline{\alpha}') \overset{(n)}{\varepsilon_{mn}^{\mathrm{aux}}}(\underline{\alpha}') + f_{ij}(\underline{\alpha}), \quad n \in \{1, 2, 3, \cdots\}.
\end{aligned} \tag{3.7}$$

We now have to answer the following questions:

(i) Does, for a fixed and sufficiently large N, the sequence $\overset{(0)}{\varepsilon}{}^{\text{aux}}_{mn}$, $\overset{(1)}{\varepsilon}{}^{\text{aux}}_{mn}$, $\overset{(2)}{\varepsilon}{}^{\text{aux}}_{mn}$, $\cdots$ converge in an appropriate norm against the solution of the system (3.1)?

As we shall show the suitable choice of material data, *i.e.*, of C^{aux}_{ijkl} is of crucial importance in this context.

After having established the convergence of the sequence mentioned before for a fixed N we are confronted with the additional problem:

(ii) Does the solution also exist for infinitely growing N and, for sufficiently large N, become independent of it?

In view of question (ii) we recall that the discrete system (3.1) was created by substituting the derivatives of the initially continuous problem by difference quotients for a fixed number, N^d, of support points. Subsequently, we have applied to the resulting discrete problem the discrete Fourier transform. As we will show question (ii) can also be answered positively.

We investigate question (i) first. The system (3.1) represents in d spatial dimensions and for N^d support points $D = 1/2d \cdot (d+1) \cdot N^d$ equations for the corresponding number of unknowns, which we combine in a vector. For example we may write in the case of two dimensions, *i.e.*, $d = 2$:

$$
\begin{aligned}
\mathbf{w} = \Big\{ & \varepsilon^{\text{aux}}_{11}(0,0), \varepsilon^{\text{aux}}_{11}(1,0), \cdots, \varepsilon^{\text{aux}}_{11}(N-1,0), \cdots, \\
& \varepsilon^{\text{aux}}_{11}(0,N-1), \varepsilon^{\text{aux}}_{11}(1,N-1), \cdots, \varepsilon^{\text{aux}}_{11}(N-1,N-1), \\
& \varepsilon^{\text{aux}}_{22}(0,0), \varepsilon^{\text{aux}}_{22}(1,0), \cdots, \varepsilon^{\text{aux}}_{22}(N-1,0), \cdots, \\
& \varepsilon^{\text{aux}}_{22}(0,N-1), \varepsilon^{\text{aux}}_{22}(1,N-1), \cdots, \varepsilon^{\text{aux}}_{22}(N-1,N-1), \\
& 2\varepsilon^{\text{aux}}_{12}(0,0), 2\varepsilon^{\text{aux}}_{12}(1,0), \cdots, 2\varepsilon^{\text{aux}}_{12}(N-1,0), \cdots, \\
& 2\varepsilon^{\text{aux}}_{12}(0,N-1), 2\varepsilon^{\text{aux}}_{12}(1,N-1), \cdots, 2\varepsilon^{\text{aux}}_{12}(N-1,N-1) \Big\}.
\end{aligned}
\tag{3.8}
$$

The components of such a vector will be indexed by means of a super index $I = \{1, 2, \cdots, D\}$. Indices of type I will be labeled using capital letters $A, B, C, \cdots$. Moreover we assign $K_{ijmn}(\underline{\alpha}, \underline{\alpha}') \to K_{AB}$ and $f_{ij}(\underline{\alpha}) \to f_A$. Thus we can now write the system (3.1) in a further simplified form that reads:

$$
w_A = \sum_{B=1}^{D} K_{AB} w_B + f_A, \qquad \text{with } A \in I. \tag{3.9}
$$

Next we refer to a statement, based on Banach's fixed-point theorem, from the textbooks by Heuser (1982), pp. 17, or Kreyszig (1978), pp. 309. If one of the numbers:

$$
q_1 = \max_{B=1}^{D} \sum_{A=1}^{D} \left| K_{AB} \right|, \quad q_2 = \sqrt{\sum_{A,B=1}^{D} \left| K_{AB} \right|^2}, \quad q_\infty = \max_{A=1}^{D} \sum_{B=1}^{D} \left| K_{AB} \right| \tag{3.10}
$$

is less than one, then the system of Equations (3.9) possesses exactly one solution. This solution can be determined by iteration and the sequence of iterates converges componentwise to the solution. It should be noted that the indices 1, 2, and ∞ refer to the corresponding metrics used during the proof, *i.e.*, to the absolute distance metric, the Euclidean metric and to the maximum metric, respectively:

$$d_1 = \sum_{A=1}^{D} \left| w_A - w'_A \right|, \quad d_2 = \left(\sum_{A=1}^{D} \left(w_A - w'_A \right)^2 \right)^{1/2}, \quad d_\infty = \max_A \left| w_A - w'_A \right|. \tag{3.11}$$

Expressed by the quantities pertinent to the current problem the first and the last of the three conditions read:

$$q_1 = \max_{\substack{m,n \in \{1,\cdots,d\} \\ \alpha'_1,\cdots,\alpha'_d = [0,\cdots,N-1]}} \left\{ \sum_{i,j \in \{1,\cdots,d\}} \left| \lambda_{ijrs} \right| \sum_{\substack{\alpha_1,\cdots,\alpha_d = \\ [0,\cdots,N-1]}} \left[\left| \beta(\alpha) k_{rsmn}(\underline{\alpha}, \underline{\alpha}') \right| \right] \right\} < 1, \tag{3.12}$$

$$q_\infty = \max_{\substack{i,j \in \{1,\cdots,d\} \\ \alpha_1,\cdots,\alpha_d = [0,\cdots,N-1]}} \left\{ \left| \beta(\alpha) \lambda_{ijrs} \right| \sum_{m,n \in \{1,\cdots,d\}} \left[\sum_{\substack{\alpha'_1,\cdots,\alpha'_d = \\ [0,\cdots,N-1]}} \left| k_{rsmn}(\underline{\alpha}, \underline{\alpha}') \right| \right] \right\} < 1, \tag{3.13}$$

which can both be conveniently evaluated using the form for $k_{rsmn}(\underline{\alpha}, \underline{\alpha}')$ presented in Equation (3.5). At this point it should already be noted that for any choice of $\underline{\alpha}'$ (in the case of Equation (3.12)) or $\underline{\alpha}$ (in the case of Equation (3.13)) the summations concerning $k_{rsmn}(\underline{\alpha}, \underline{\alpha}')$ will lead to the same result. This is because of periodicity conditions, which also apply to $A^{\mathrm{aux}}_{ijmn}(\underline{\alpha} - \underline{\alpha}')$ and allow these quantities to be mapped directly onto $A^{\mathrm{aux}}_{ijmn}(\underline{\alpha})$ and $A^{\mathrm{aux}}_{ijmn}(\underline{\alpha}')$, respectively.

For the numerical evaluation of the second condition it is advantageous not to use the form shown in Equation (3.6), *i.e.*, not to return from Fourier space but to write instead:

$$q_2^2 = \frac{1}{N^{2d}} \lambda_{ijrs} \overline{\lambda_{ijuv}} \times \tag{3.14}$$

$$\sum_{\underline{\alpha}} \left\{ \beta(\underline{\alpha}) \overline{\beta(\underline{\alpha})} \sum_{\underline{s}} \sum_{\underline{s}'} \left[\hat{A}^{\mathrm{aux}}_{rsmn}(\underline{s}) \overline{\hat{A}^{\mathrm{aux}}_{uvmn}(\underline{s}')} \sum_{\underline{\alpha}'} \left[\exp\left(\mathrm{i} \frac{2\pi}{N} (\underline{\alpha}' - \underline{\alpha}) \cdot (\underline{s} - \underline{s}') \right) \right] \right] \right\} =$$

$$\frac{\lambda_{ijrs} \lambda_{ijuv}}{N^d} \sum_{\underline{\alpha}} \left\{ \beta^2(\underline{\alpha}) \sum_{\underline{s}} \sum_{\underline{s}'} \left[\hat{A}^{\mathrm{aux}}_{rsmn}(\underline{s}) \hat{A}^{\mathrm{aux}}_{uvmn}(\underline{s}') \exp\left(\mathrm{i} \frac{2\pi}{N} (\underline{\alpha}' - \underline{\alpha}) \cdot (\underline{s} - \underline{s}') \right) \delta_{\underline{s},\underline{s}'} \right] \right\},$$

where bars denote complex conjugates. In this expression we have invoked the geometric series:

$$\sum_{\alpha=0}^{N-1} q^\alpha = \frac{1 - q^N}{1 - q}, \quad q \neq 1, \tag{3.15}$$

where:

$$q = \exp\left(\mathrm{i} \frac{2\pi}{N} (s' - s) \right) \tag{3.16}$$

to obtain the following relation:

$$\sum_{\underline{\alpha}'} \left[\exp\left(\mathrm{i}\frac{2\pi}{N}\underline{\alpha} \cdot (\underline{s} - \underline{s}') \right) \right] = N^d \delta_{s_1 s_1{}'} \cdots \delta_{s_d s_d{}'} = N^d \delta_{\underline{s}\,\underline{s}'}. \tag{3.17}$$

Consequently, we finally obtain the following expression to numerically evaluate and use for checking the validity of the inequality:

$$q_2 = \sqrt{\sum_{\underline{\alpha}} (\beta^2(\underline{\alpha})) \frac{\lambda_{ijrs}\lambda_{ijuv}}{N^d} \sum_{\underline{s}} \left(\hat{A}^{\mathrm{aux}}_{rsmn}(\underline{s}) \hat{A}^{\mathrm{aux}}_{uvmn}(\underline{s}) \right)} < 1. \tag{3.18}$$

We will evaluate and discuss the three inequalities in the next section. However, in order to anticipate a main result it should be mentioned now that only for the first condition the convergence criterion is observed to be fulfilled, *i.e.*, $q_1 < 1$. It should be noted that even for this case its fulfillment depends strongly on the choice of the constants C^{aux}_{ijkl}.

Next we turn to the question what happens if we let the number N, which so far has been kept fixed, grow indefinitely. Note that in the inequalities only the quantities $k_{mnrs}(\underline{\alpha}, \underline{\alpha}')$ depend upon N, and therefore we write $k^N_{mnrs}(\underline{\alpha}, \underline{\alpha}')$. An examination of the explicit form of these quantities results in the existence of a limit element according to:

$$\lim_{N \to \infty} k^N_{mnrs}(\underline{\alpha}, \underline{\alpha}') = k^\infty_{mnrs}(\underline{\alpha}, \underline{\alpha}') < \infty. \tag{3.19}$$

In the case of q_1 this condition is already satisfied surprisingly well for $N \geq 128$, as will also be documented in the next section.

Finally we may write for the error bounds involved with the three numbers mentioned above (*cf.*, Kreyszig, 1978, pg. 309):

$$d_p\big(w_A^{(m)}, w_A\big) \leq \frac{q_p^m}{1 - q_p} d_p\big(w_A^{(0)}, w_A^{(1)}\big), \tag{3.20}$$

where w_A is the correct solution to the problem, $w_A^{(m)}$ refers to the m-th iteration and d_p, $p = 1, 2, \infty$ refers to the metrics shown in Equation (3.11).

4 Results

If we now refer to Equations (3.12), (3.13), (3.18) of the previous section, we can see that by virtue of A^{aux}_{ijkl} or $\hat{A}^{\mathrm{aux}}_{ijkl}$ the choice of the $\underline{\underline{C}}^{\mathrm{aux}}$ tensor will have a marked effect on the convergence of the system due to its use in the formulation of Equation (2.7) and of Equations (2.14), (2.15). Indeed, an appropriate choice of this tensor is the single most important factor in a successful analysis and although, in theory, it can take any value, we restricted ourselves in Table 2.1 to three cases that immediately come to mind.

In case 1 the auxiliary stiffness was chosen to be the stiffness of the matrix. In fact, this case is the "native" choice for treatment of inclusions softer than the surrounding matrix. Previous empirical computational studies (Müller, 1996) have shown that in this case convergence seems to be guaranteed as long as the matrix is stiffer than the inclusion. This is also demonstrated by the first column of insets in Figure 4.1. In general, Figure 4.1 shows the strain field ε_{11} of a single circular inclusion subjected to a remotely imposed strain $\varepsilon_{11}^0 = 0.1\%$. The local strain has been plotted for the three choices of auxiliary tensor after twelve iterations (for which, as will be demonstrated shortly, convergence has been reached). The effect of the divergence of the solution on the analysis can clearly be seen where the shape of the strain field appears distorted, and the magnitudes of the solution become unrealistically high.

Similarly, case 2, where the stiffness of the inclusion takes over the role of the auxiliary stiffness, allows handling of rigid inclusions in soft matrices. "Experience" has shown that convergence seems to be guaranteed provided the stiffness of the inclusion is greater than the stiffness of the matrix. This is illustrated by the second column of insets in Figure 4.1.

Finally, in case 3 the auxiliary stiffness was chosen to become the average of both stiffnesses. In a certain sense this is a "generic" choice which seems to guarantee convergence for any degree of mismatch between the inclusion and the matrix (see the insets in the third row of Figure 4.1), although at a slower rate (this will be discussed in a later section). It should be pointed out that this choice is recommended in the papers by Moulinec and Suquet (1998), and Michel *et al.* (1999, 2001).

If we refer again to Equations (3.12), (3.13), (3.18), we can see that the second parameter affecting the convergence is the factor $\beta(\underline{\alpha})$, which was introduced in Section 2. In fact, during the numerical evaluation of Equations (3.13) and (3.18), the summation with respect to this very factor, *i.e.*, q_2 and q_∞, will always result in values greater one for all choices of stiffness but those extremely close to $E^+/E^- = 1$. For conciseness we refrain from presenting explicit data and refer the reader to the corresponding equations if confirmation is desired.

In contrast to that $\beta(\underline{\alpha})$ has a beneficial influence while calculating q_1 according to Equation (3.12). Suggestively speaking it has a "screening effect" and blocks a huge amount of otherwise positive contributions. Clearly this benevolent feature diminishes with increasing volume fraction of the inclusion. To illustrate all these effects we first refer to Table 4.1 and note that the volume fraction is given by:

$$v_f = \frac{\text{area of inclusion}}{\text{area of RVE}}. \tag{4.1}$$

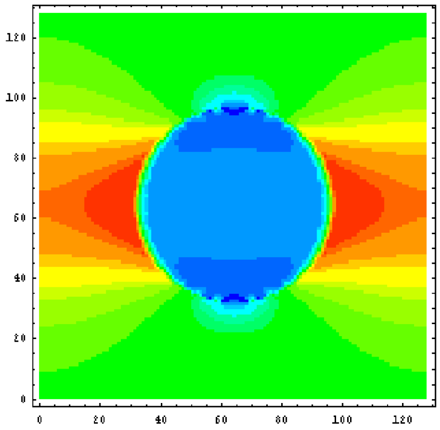

correct, “native” choice

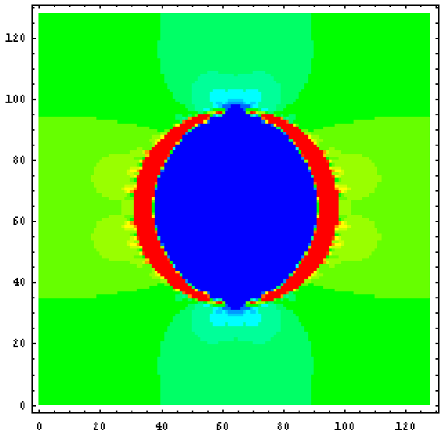

incorrect, divergent choice

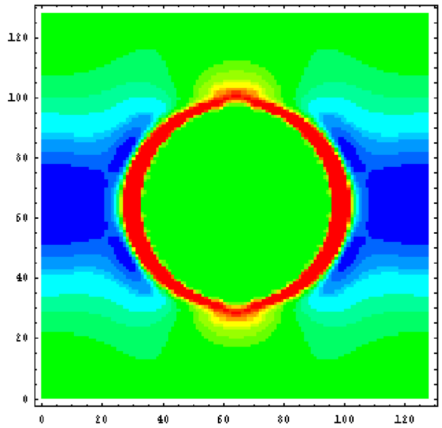

incorrect, “divergent” choice

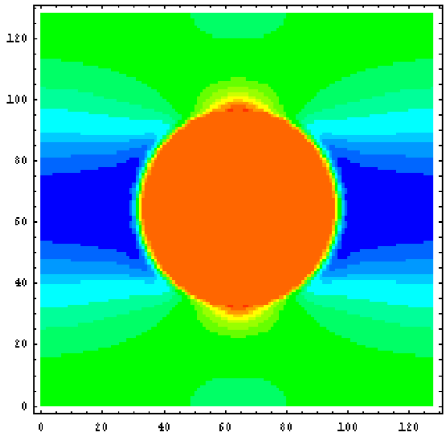

correct, “generic” choice

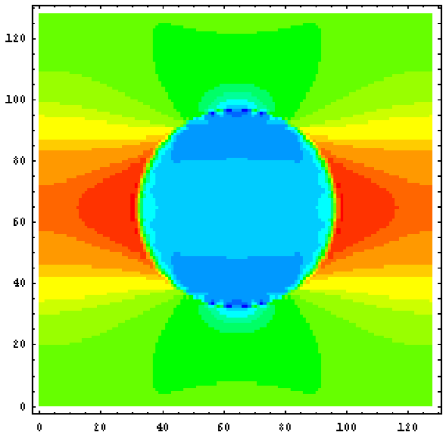

correct, “generic” choice

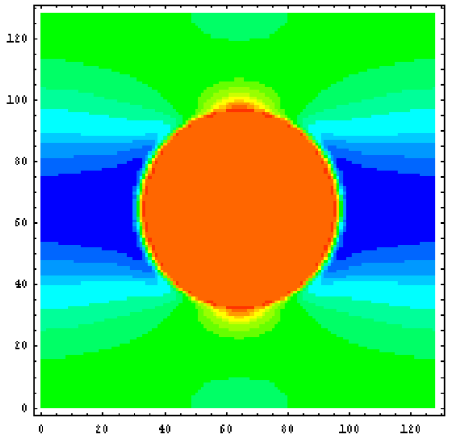

correct, “generic” choice

Figure 4.1 ε_{11} for (left column) $E^+/E^- = 10,\ \nu^+ = 0.3,\ \nu^- = 0.3,\ v_f = 0.2$; (right column): $E^+/E^- = 0.1,\ \nu^+ = 0.3,\ \nu^- = 0.3,\ v_f = 0.2$.

$\underline{\underline{C}}^{\text{aux}}$	$\beta(\underline{\alpha})$	$\sum_{\underline{\alpha}} \beta(\underline{\alpha})$	$\frac{1}{N^2} \sum_{\underline{\alpha}} \beta^2(\underline{\alpha})$
$\underline{\underline{C}}^{+}$	θ	$N^2 v_f$	v_f
$\underline{\underline{C}}^{-}$	$\theta - 1$	$N^2(v_f - 1)$	$1 - v_f$
$\frac{1}{2}(\underline{\underline{C}}^{+} + \underline{\underline{C}}^{-})$	$\frac{1}{2}(2\theta - 1)$	$\frac{1}{2}N^2(2v_f - 1)$	$\frac{1}{4}$

Table 4.1 The factor $\beta(\underline{\alpha})$ and result of summation in real space for different choices of $\underline{\underline{C}}^{\text{aux}}$.

Next we draw the attention to the sequence of pictures shown in Figure 4.2 where all k_{ijkl}'s relevant for 2D-simulations are depicted. Obviously, the smaller values can be found in the vicinity of the center, *i.e.*, for $\alpha_1 = \alpha_2 = N/2$. Note that the values for k_{ijkl} depend slightly on the number of discretization points, N. However, at least for points close to the center convergence is achieved very rapidly as indicated by the sequence shown in Figure 4.3. It should also be pointed out that in the case of isotropic materials for a fixed Poisson's ratio, ν^{aux}, k_{ijkl} does not depend on the choice of E^{aux}.

It now becomes straightforward to use Equation (3.12) to calculate estimates of the "convergence radii" q_1 for several different volume fraction and material mismatch configurations, and it can be seen that it is not necessary to start the Neumann iteration in order to get an estimate of the convergence criteria. The advantage of employing this method as a precursor to any analysis becomes obvious since it does not now require that the analysis be started with the possibility that the parameters chosen will be non-convergent. Moreover, the quantities in the calculation are reusable in the Neumann iteration ensuring maximum efficiency. This is especially important on large-scale analyses where the determination of convergence in the early stages of the analysis can translate to large overall time-savings.

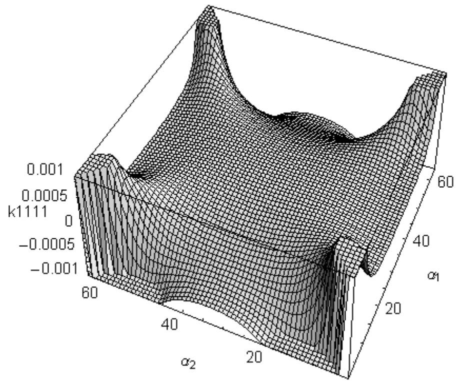
0.001
0.0005
k1111
0
−0.0005
−0.001
60
40
α_2
20
60
40
α_1
20
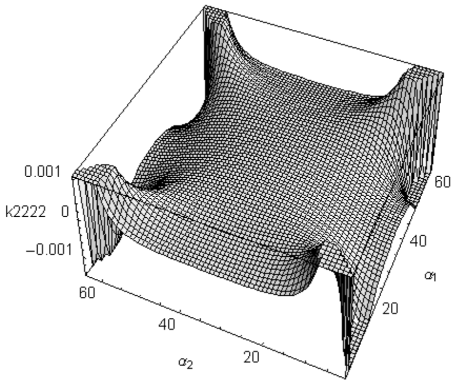
0.001
k2222
0
−0.001
60
40
α_2
20
60
40
α_1
20
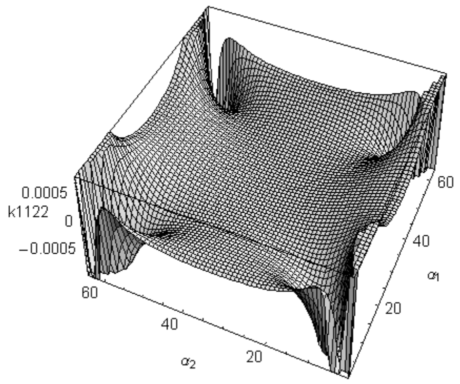
0.0005
k1122
0
−0.0005
60
40
α_2
20
60
40
α_1
20
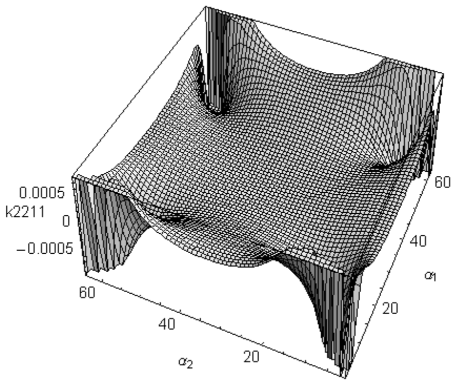
0.0005
k2211
0
−0.0005
60
40
α_2
20
60
40
α_1
20
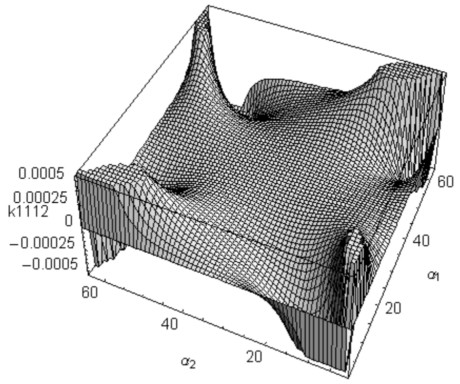
0.0005
0.00025
k1112
0
−0.00025
−0.0005
60
40
α_2
20
60
40
α_1
20
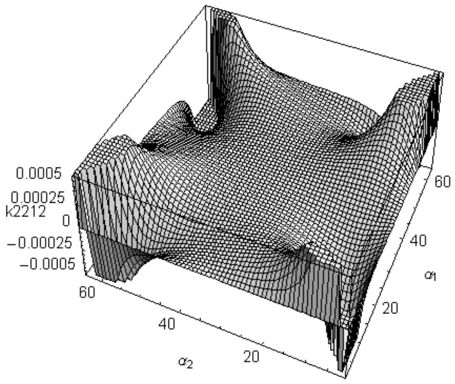
0.0005
0.00025
k2212
0
−0.00025
−0.0005
60
40
α_2
20
60
40
α_1
20
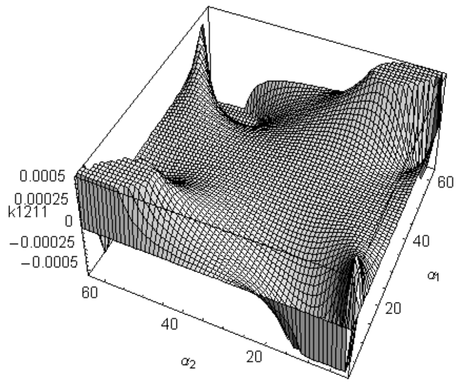
0.0005
0.00025
k1211
0
−0.00025
−0.0005
60
40
α_2
20
60
40
α_1
20
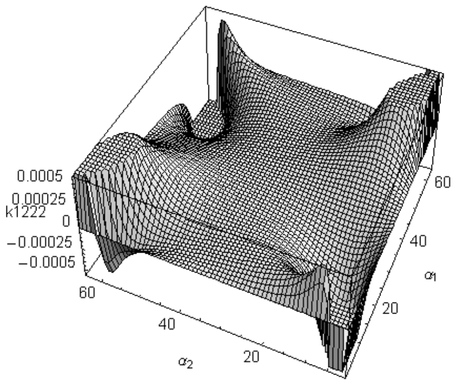
0.0005
0.00025
k1222
0
−0.00025
−0.0005
60
40
α_2
20
60
40
α_1
20

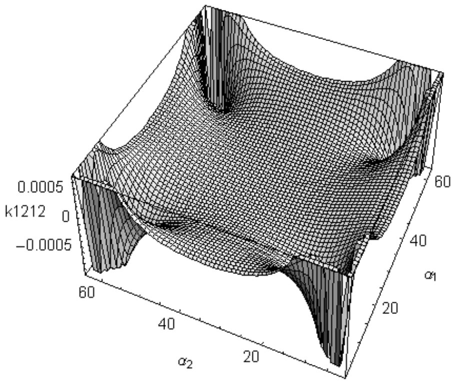

Figure 4.2: All k_{ijkl}'s relevant for 2D-simulations $(N = 64, \nu^{\text{aux}} = 0.3)$.

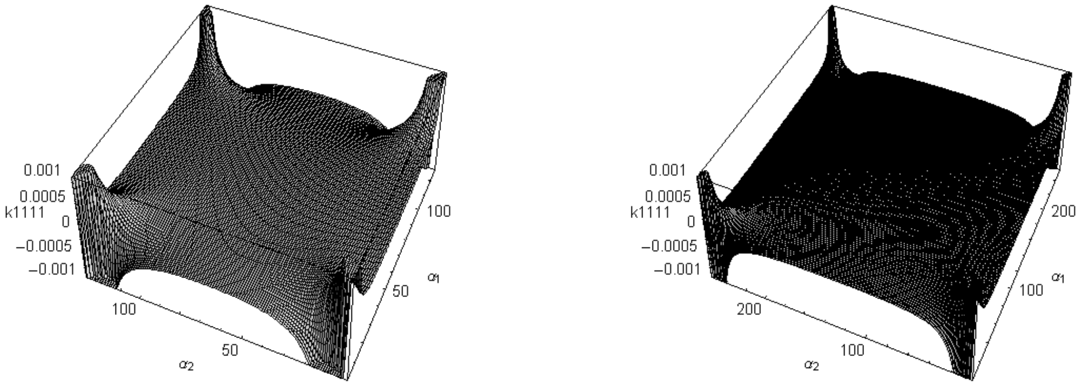

Figure 4.3: k_{1111} for $N = 128$ and $N = 256(\nu^{\text{aux}} = 0.3)$.

The sequence presented in Figure 4.4 shows plots for the choice $\underline{\underline{C}}^{\text{aux}} = \underline{\underline{C}}^{+}$ and various volume fractions on the "convergence radius" q_1 as a function of numbers of pixels, N. Note that the system is assumed to be in a state of plane strain, and that we may safely assume any out-of-plane contributions from any quantity in the analysis will still result in a solution that is confined to two dimensions and can therefore be ignored. The proof of this lemma is provided in the appendix, specifically for the quantity $\hat{A}^{\text{aux}}_{klmn}$, which is the only quantity in the analysis that is not intrinsically confined to the xy-plane. The plots show several features worthy of comment, as follows:

- Convergence of q_1 is achieved very rapidly, even at high volume fractions.
- For low to medium volume fractions q_1 stays below 1 provided the matrix is stiffer than the inclusion, as anticipated.
- For low to medium volume fractions convergence can also be proven for matrix stiffnesses $0.5 \leq E^{+}/E^{-} \leq 1$. In fact this behavior had been observed before (Müller, 1996). It is fair to say that many common engineering materials

fall into this class. However, composite materials with very high ratios of mismatch do sometimes exist, such as, for example, steel inclusions embedded in an Araldite matrix (*e.g.*, $E^+/E^- \approx 0.01$), and were studied in the same paper by Müller.

- At high volume fractions ($v_f = 0.6$) convergence can explicitly be demonstrated only for matrix stiffnesses $1 \leq E^+/E^- \leq 5$.
- Also note that for the trivial case where $E^+/E^- = 1$ and $\nu^+ = \nu^-$ we are looking at an elastically homogeneous material and that therefore the convergence radius is identically zero.

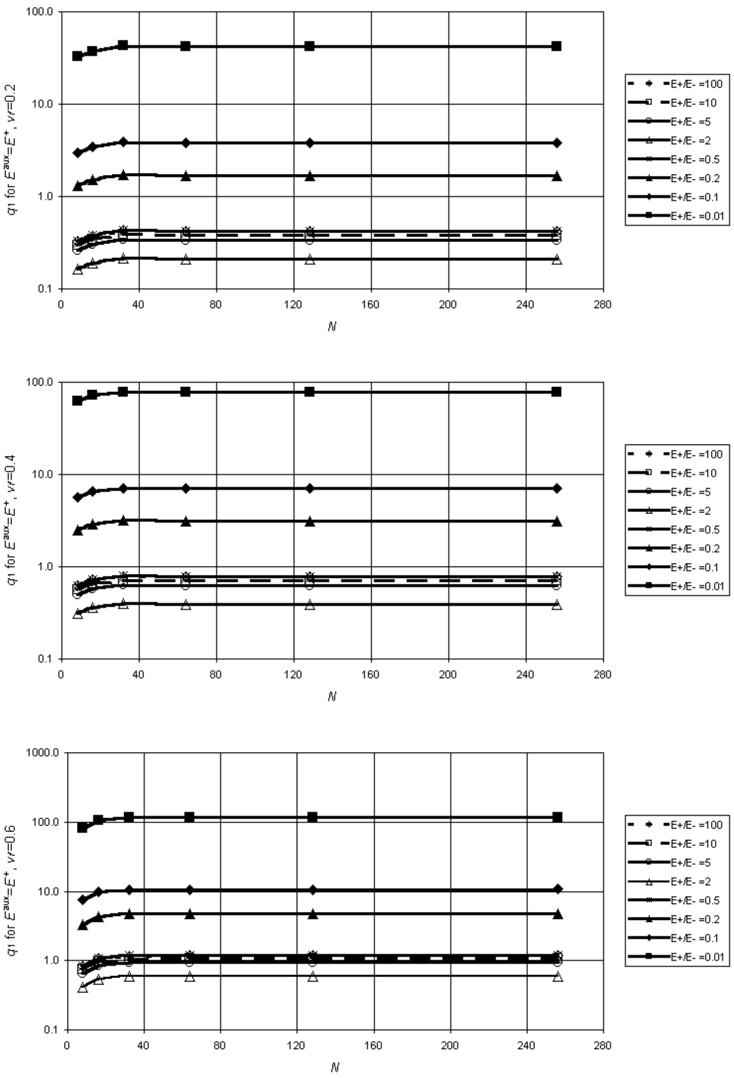

Figure 4.4: $\underline{\underline{C}}^{\text{aux}} = \underline{\underline{C}}^+$: q_1 as a function of pixels, N, at three different volume fractions, $v_f = 0.2, 0.4, 0.6$ ($\nu^+ = \nu^- = 0.3$).

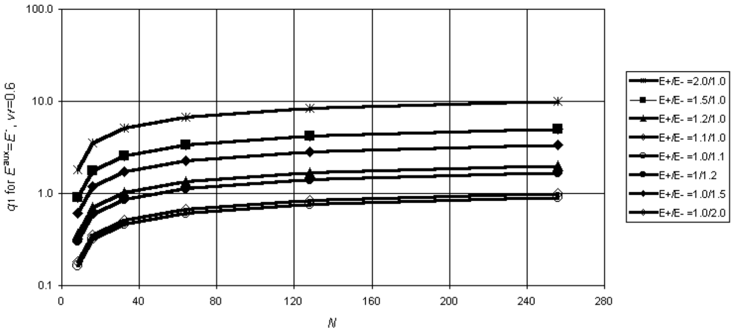

Figure 4.5: $\underline{\underline{C}}^{\text{aux}} = \underline{\underline{C}}^{-}$: q_1 as a function of pixels, N, at three different volume fractions, $v_f = 0.6$ ($\nu^+ = \nu^- = 0.3$).

Figure 4.5 focuses on the choice $\underline{\underline{C}}^{\text{aux}} = \underline{\underline{C}}^{-}$. Due to the fact that $\beta(\underline{\alpha})$ is zero in the center and one in the outside regions large values of k_{ijkl} contribute pushing q_1 easily above the critical limit. Consequently, convergence could be proven explicitly only for stiffness ratios $1/1.1 \leq E^+/E^- \leq 1.1/1$. However, it should be noted that this does not exclude the possibility for convergence beyond these limits, in particular for ratios of stiffness below one, for which convergence has been demonstrated empirically (*cf.*, Figure 4.1). Also note that because of the slower convergence of k_{ijkl} outside of the center $\alpha_1 = \alpha_2 = N/2$ the convergence of q_1 is retarded as well.

The behavior of q_1 for the generic type of auxiliary tensor (*i.e.*, the third choice shown in Table 4.1, $\underline{\underline{C}}^{\text{aux}} = 0.5(\underline{\underline{C}}^{+} = \underline{\underline{C}}^{-})$) is illustrated in Figure 4.6. Since $|\beta(\underline{\alpha})| = 0.5$ for all possible values of $\underline{\alpha}$ within the RVE we conclude that the numerical results for q_1 are independent of the volume fraction chosen. Evidently convergence, based on values $q_1 < 1$, can explicitly be demonstrated only for $1/1.2 \leq E^+/E^- \leq 1.2/1$. The reason for the relatively small extension beyond the purely homogeneous case is the full summation, *i.e.*, positive contributions toward q_1, from *all* the points within the RVE, including those from the out-of-center points, which are particularly large as shown in Figure 4.1. Nevertheless, in comparison with the previous case, *i.e.*, the behavior of q_1 for the choice $\underline{\underline{C}}^{\text{aux}} = \underline{\underline{C}}^{-}$, is slightly better, in particular in view of the fact that the present results are independent of the volume fraction.

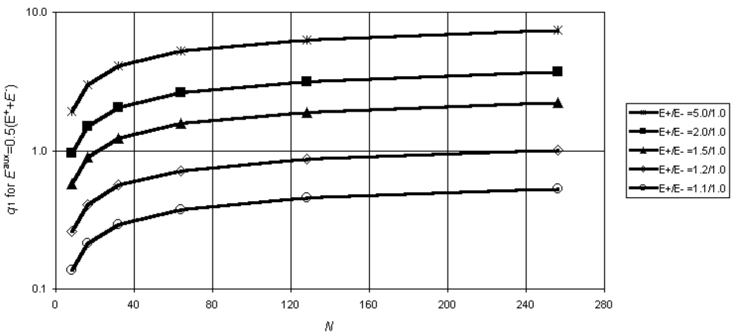

Figure 4.6: $\underline{\underline{C}}^{\text{aux}} = 0.5(\underline{\underline{C}}^{+} = \underline{\underline{C}}^{-})$: q_1 as a function of pixels, N.

Figures 4.7 and 4.8 are the counterparts to Figure 4.4_1 when different Poisson's ratios are used for the inclusion and for the matrix, namely $\nu^+ = 0.4$, $\nu^- = 0.1$ and $\nu^+ = 0.1$, $\nu^- = 0.4$, respectively. Generally speaking, different Poisson's ratios seem to impede convergence. Moreover, for the same ratio of stiffness, the convergence radii of both choices are clearly not identical. This is attributable to different lateral contraction constraints depending on the system geometry, *i.e.*, laterally stiff inclusion or shell. This implies that the not only the level of elastic mismatch and volume fraction but also the *shape* of the inclusion will affect the convergence radius, although this is not studied in any detail at this time.

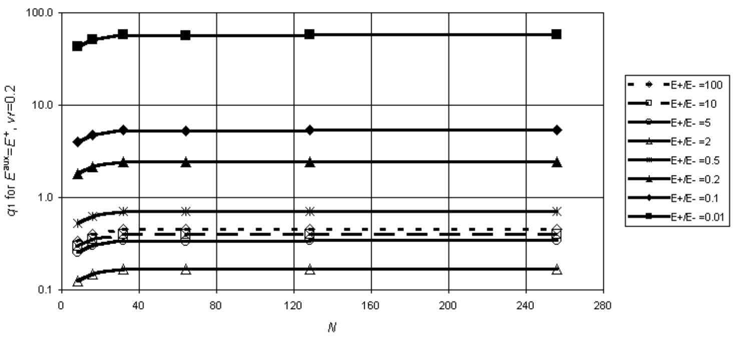

Figure 4.7: $\underline{\underline{C}}^{\text{aux}} = \underline{\underline{C}}^{+}$: q_1 as a function of pixels, N ($\upsilon_f = 0.2$, $\nu^+ = 0.4$, $\nu^- = 0.1$).

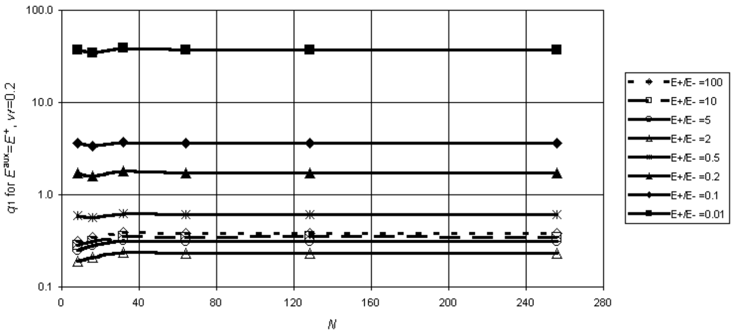

Figure 4.8: $\underline{\underline{C}}^{\text{aux}} = \underline{\underline{C}}^{+}$: q_1 as a function of pixels, N ($\upsilon_f = 0.2$, $\nu^+ = 0.1$, $\nu^- = 0.4$).

An interesting special case with physical relevance is the void, and is of interest particularly when modeling porous materials (Latella and Liu, 2000) or in the study of elliptical holes or Griffith cracks (Herrmann *et al.*, 1999). Figures 4.4/7/8 indicate (for $E^+/E^- \gg 1$) that the presented approach is capable to handle such cases. In this context it should also be noted that Moulinec and Suquet (1998) report no convergence for "infinite contrast" between the constituents (*i.e.*, for rigid inclusions as well as voids). However, it must also be noted that their method is based on a continuous Green's operator solution for the elastic problem and differs in this respect from our numerical scheme (2.24) which is based on discrete finite differences in Fourier space shown in Equations (2.11)-(2.13).

5 Relative error of the Neumann iteration

It is, of course, of interest to us to know the relative error of the current value of the Neumann iteration since it is not computationally efficient to carry out more than the necessary number of iterations for this numerical scheme. Indeed, since the execution of this iteration is generally the most intensive part of the numerical simulation, an understanding of this value can make significant differences to the execution time of the entire simulation.

Explicit relations for computing the relative error of the solution of equations have already been provided in Equations (3.11/3.20). These will now be evaluated for the case $p = 1, \underline{\underline{C}}^{\text{aux}} = \underline{\underline{C}}^{+}$. The sequence in Figure 5.1 shows the logarithm of the relative error, $q_1^m/(1-q_1)$, plotted as a function of iteration number, m, for different stiffness ratios and the various choices of Poisson's ratio that were used before. As before a circular inclusion corresponding to a fixed volume fraction, $v_f = 0.2$, was chosen to obtain the results. Generally speaking, the following conclusions can be drawn:

- the stiffer the matrix, the slower the convergence speed; this is in particular true for the case of holes, *i.e.*, when the stiffness ratio approaches $E^+/E^- = \infty$;
- for the convergent case $E^+/E^- = 0.5$, which is "non-native" to the choice $\underline{\underline{C}}^{\text{aux}} = \underline{\underline{C}}^{+}$, a drastic reduction in convergence speed can be observed;
- different choices of Poisson's ratio lead to a decrease in convergence speed for most choices of stiffness ratio with the exception of relatively small ones.

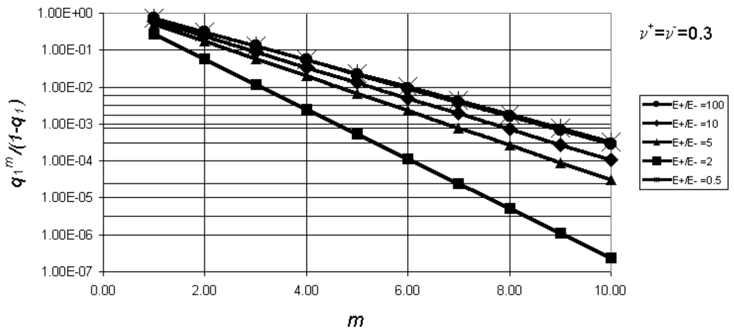

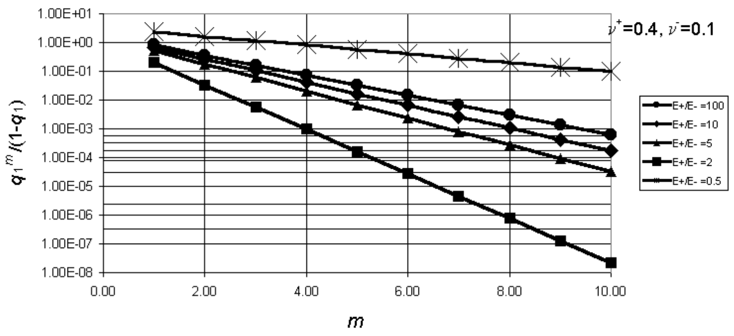

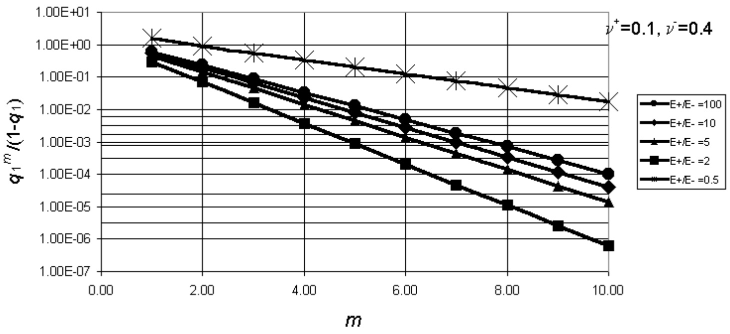

Figure 5.1: Error bound ratio, $q_1^m/(1-q_1)$, as a function of number of iterations, m, for various choices of Poisson's ratios ($v_f = 0.2$).

This result would seem to suggest that perhaps a more computationally efficient strategy for increasing the speed of convergence would be to calculate the convergence radius for each of the three choices of stiffness tensor. Furthermore, it would be sensible to assume at this stage that the rule of mixtures could be employed to optimize the choice of the auxiliary stiffness tensor at a pre-analysis stage, in order that the execution time of the numerical procedure could be reduced, such as:

$$\underline{\underline{C}}^{\text{aux}} = v_f \underline{\underline{C}}^{-} + \left(1 - v_f\right) \underline{\underline{C}}^{+}. \tag{5.1}$$

However, a detailed analysis of this suggestion is left to future research.

6 Conclusions and outlook

A local stress/strain analysis for elastically highly heterogeneous bodies ("composites") has been performed on the basis of Eshelby's "equivalent inclusion technique". The associated discrete version of a Fredholm equation of the second-type has been solved numerically using Discrete Fourier Transforms (DFT) in combination with a Neumann iteration scheme. Convergence issues in context with the choice of extremely different stiffness ratios for a circular inclusion and a surrounding matrix have been addressed and investigated. Moreover, it was shown that for a decreasing convergence radius convergence of the solution may occur at a faster rate. It should finally be pointed out that the presented method can be used to study elastically heterogeneous materials showing a much more complicated substructure and, due to its overall efficiency, allows the study of micromorphological evolution of such structures. This has recently been demonstrated in Dreyer and Müller (2000) for a computer simulation of the phase separation and coarsening phenomenon observed in eutectic SnPb solders.

References

[1] Bronstein, I.N. and Semendjajew, K.A. 1976 *Taschenbuch der Mathematik*. Verlag Harri Deutsch, 16. Auflage, Zürich, Frankfurt/Main, Thun.

[2] Brown, C.M. and Müller, W.H. 2000 *An Approximate Analytical Solution for the Stresses and Strains in an Eigenstrained Cubic Material*, Acta Mechanica, **146** (3-4), pp. 151-167.

[3] Christensen, R.M. 1979 *Mechanics of Composite Materials.* Fl. USA: Krieger Publishing Company.

[4] Dreyer, W., and Müller, W.H. 2000 *A Study of the Coarsening in Pb/Sn Solders*, Int. J. Solids and Structures, **37** (28), pp. 3841-3871.

[5] Hashin, Z. 1962 *The Elastic Moduli of Heterogeneous Materials*, Journal of Applied Mechanics. **29**, pp. 143-150.

[6] Hashin, Z. 1964 *Theory of Mechanical Behavior of Heterogeneous Media*, Applied Mechanics Reviews, **17** (1), pp. 1-9.

[7] Hazotte, A., Grosdidier, T., and Denis, S. 1996 *Gamma' Precipitate splitting in nickel-based superalloys: A 3-D finite element analysis*, Scripta Mater., **34** (4) pp. 601-608.

[8] Herrmann, K.P., Müller, W.H., and Neumann, S. 1999 *Linear and Elastic-Plastic Fracture Mechanics Revisited by use of Fourier Transforms - Theory and Application*, Computational Materials Science, **16**, pp. 186-196.

[9] Heuser, H.G. 1982 *Functional Analysis*, John Wiley and Sons, Chichester, New York, Brisbane, Toronto Singapore.

[10] Holmbom, A., Persson, L-E., and Svanstedt, N. 1992 *A Homogenization Procedure for Computing Effective Moduli and Microstresses in Elastic Composite Materials*, Composites Engineering, **2** (4), pp. 249-259.

[11] Kreyszig, E. 1978 *Introductory Functional Analysis with Applications.* John Wiley & Sons, New York.

[12] Latella, B.A., and Liu, T. 2000 *Performance Characteristics of Porous Alumina in Ceramic Structures*, J. Aust. Ceram. Soc., **36** (92), pp. 13–21.

[13] Lukassen, D., Persson, L-E., and Wall, P. 1995 *Some Engineering and Mathematical Aspects of the Homogenization Method*, Composites Engineering **5** (5), pp. 519-531.

[14] Michel, J.C., Moulinec, H., and Suquet, P. 1999 *Effective Properties of Composite Materials with Periodic Microstructure: A Computational Approach*, Comput. Methods Appl. Mech. Engrg., **192** (1-4), pp. 109-143.

[15] MOISEIWITSCH, B.L. 1977 *Integral Equations.* New York, USA: Longman Group Ltd.

[16] MOULINEC, H., AND SUQUET, P. 1995 *A FFT-based Numerical Method for Computing the Mechanical Properties of Composites from Images of their Microstructures.* IUTAM Symposium on Microstructure-Property Interactions in Composite Materials, pp. 235-246.

[17] MOULINEC, H., AND SUQUET, P. 1998 *A Numerical Method for Computing the Overall Response of Nonlinear Composites with Complex Microstructure*, Comp. Meth. Appl. Mech. Engng. **157** (1-2), pp. 69-94.

[18] MÜLLER, W.H. 1996 *Mathematical vs. Experimental Stress Analysis of Inhomogeneities in Solids.*, Journal de Physique IV., Colloque C1, supplément au Journal de Physique III, Volume 6, pp. C1-139 – C1-148.

[19] MURA, T. 1987 *Micromechanics of Defects in Solids.* Second revised edition. Dordrecht, The Netherlands: Martinus Nijhoff Publishers.

[20] PIPKIN, A.C. 1991 *A Course on Integral Equations.* New York: Springer-Verlag.

[21] PORTER, D., AND STIRLING, D.S.G. 1990 *Integral Equations: A Practical Treatment from Spectral Theory to Applications.* Cambridge: Cambridge University Press.

Appendix. Proof of disappearance of out-of-plane components of $\hat{A}^{\mathbf{aux}}_{klmn}$

The purpose of this appendix is to demonstrate that within the context of the current problem all components of the quantity $\hat{A}^{\mathrm{aux}}_{klmn}$ that are out-of-plane, *i.e.*, those for which at least one of the four indices is equal to 3, will disappear due to the imposed condition of plane strain. It should be noted that the complexity of this quantity does not allow us to simply dismiss the out-of-plane components due to the inherently three-dimensional nature of the stiffness tensor from which it is partially constructed.

We shall begin the proof by recalling the generalized form of the Neumann iteration, introduced as Equation (2.24):

$$\begin{aligned} \varepsilon^{\mathrm{aux}}_{rs}(\underline{\alpha}) \;=\;& \beta(\underline{\alpha})\left(C^{\mathrm{aux}}\right)^{-1}_{rsij}\left(C^{+}_{ijkl}-C^{-}_{ijkl}\right)\left[Y^{-1}\left(\hat{A}^{\mathrm{aux}}_{klmn}(\underline{s})Y\left(\varepsilon^{\mathrm{aux}}_{mn}(\underline{\alpha}')\right)\right)\right]+ \\ & \beta(\underline{\alpha})\left(C^{\mathrm{aux}}\right)^{-1}_{rsij}\left(C^{+}_{ijkl}-C^{-}_{ijkl}\right)\left[Y^{-1}\left(\hat{A}^{\mathrm{aux}}_{klmn}(\underline{s})\hat{\varepsilon}^{*}_{mn}(\underline{s})\right)+\varepsilon^{0}_{kl}-\varepsilon^{*}_{kl}\right]. \end{aligned} \tag{A.1}$$

Since the quantities present in the above equation were introduced previously, we will dispense with a full discussion of their origin and instead introduce immediately the form required to hold for the following strain tensors[3] ($\varepsilon_{op}, \varepsilon^*_{op}, \varepsilon^0_{op}$):

$$\varepsilon_{op} = \begin{pmatrix} \varepsilon_{11} & \varepsilon_{12} & 0 \\ \varepsilon_{12} & \varepsilon_{22} & 0 \\ 0 & 0 & 0 \end{pmatrix}. \tag{A.2}$$

Clearly this tensor form will also remain relevant for respective Fourier transformed quantities, denoted where appropriate above by a circumflex and all of which are all similarly subject to plane-strain conditions.

It is straightforward to show that the application of this plane strain condition will force indices r, s, m and n in Equation (A.1) to be defined only when they correspond to values that lie within the (x, y)-plane in a Cartesian co-ordinate system (*i.e.*, $r, s, m, n \in \{1, 2\}$). Obviously, with reference to Equation (A.1) this limits the indices m, n in $\hat{A}_{klmn}$ to $\{1, 2\}$. This condition does not, however, automatically confine the whole this quantity to two dimensions, so it becomes necessary now to explicitly specify and investigate its components, given by:

$$\hat{A}_{klmn} = \frac{1}{2}\left(\xi_k M^{-1}_{lj} + \xi_l M^{-1}_{kj}\right) C_{ijmn}\xi_i. \tag{A.3}$$

We shall, for the moment, turn our attention exclusively to the ξ_p of the above equation, and recall that they are defined as:

$$\xi_p = -\mathrm{i}\frac{1}{h}\sin\left(\frac{2\pi}{N}s_p\right), \tag{A.4}$$

where $\mathrm{i} = \sqrt{-1}$, N is the number of discretization points per dimension, h is the mesh spacing and s_p represents the discrete position vector in Fourier space.

If we now remember that due to the formulation of the problem, we require the position vector to be defined exclusively co-planar to the strain such that

$$s_p \in \{0, 1, \cdots, N-1\}, \quad p \in \{1, 2\}. \tag{A.5}$$

It then becomes evident that Equation (A.4) can be represented in vector form as:

$$\xi_p = \begin{bmatrix} \xi_1 \\ \xi_2 \\ 0 \end{bmatrix}, \tag{A.6}$$

a result which allows us by reference to Equation (A.3) to require now that $j \in \{1, 2\}$.

[3]Note: Where possible the unbound indices o, p, u or v have been used throughout this section when required to avoid confusion with bound indices within the problem that are pertinent to the argument.

By recourse to Equation (A.3), it can clearly be seen that there is a potential for out of plane contributions arising from the M_{ou}^{-1} matrix and in order to prove that these will not occur we recall that:

$$M_{ou} = C_{opuv}\xi_{pv}, \tag{A.7}$$

and that for isotropic elastic media:

$$C_{opuv} = \lambda\delta_{op}\delta_{uv} + \mu\big(\delta_{ou}\delta_{pv} + \delta_{ov}\delta_{pu}\big). \tag{A.8}$$

Remaining aware of the tri-dimensionality of the tensor C_{opuv}, we refer to the definition of the ξ_{pv} matrices, given by[4]:

$$\xi_{\underline{p}\underline{p}} = \frac{2}{h^2}\left(\cos\left(\frac{2\pi}{N}s_p\right) - 1\right), \tag{A.9}$$

and

$$\xi_{pv} = \frac{1}{2h^2}\left(\cos\left(\frac{2\pi}{N}(s_p + s_v)\right) - \cos\left(\frac{2\pi}{N}(s_p - s_v)\right)\right), \quad p \neq v. \tag{A.10}$$

We make use again of Equation (A.5) applied to Equations (A.9–A.10), and after appropriate substitution of Equations (A.8–A.10) into Equation (A.7) and by evaluation for the isotropic case using the Mathematica® package, we arrive at the following result:

$$M_{ou}^{-1} = \begin{pmatrix} M_{11}^{-1} & M_{12}^{-1} & 0 \\ M_{12}^{-1} & M_{22}^{-1} & 0 \\ 0 & 0 & M_{33}^{-1} \end{pmatrix} \tag{A.11}$$

By inspection of Equation (A.3), we can see now that no out of plane contribution will arise due to the fact that $\xi_3 = 0$ and that $M_{3u}^{-1} = M_{u3}^{-1} \equiv 0$, with respect to indices k and l and subject to $u \in \{1, 2\}$. We can therefore conclude that indices k and l and therefore the quantity $\hat{A}_{klmn}$ be confined to two dimensions.

[4]The underlined index indicates that the Einstein convention does not apply in this case.